

# Enhanced Production of Neutron-Rich Rare Isotopes in the Reaction of 25 MeV/nucleon $^{86}\text{Kr}$ on $^{64}\text{Ni}$

G.A. Souliotis, M. Veselsky, G. Chubarian, L. Trache, A. Keksis, E. Martin, A. Ruangma, E. Winchester, and S. J. Yennello.

*Cyclotron Institute, Texas A&M University, College Station, TX 77843*

---

## Abstract

The cross sections and velocity distributions of projectile-like fragments from the reaction of 25 MeV/nucleon  $^{86}\text{Kr} + ^{64}\text{Ni}$  have been measured using the MARS recoil separator at Texas A&M, with special emphasis on the neutron rich isotopes. Proton-removal and neutron pick-up isotopes have been observed with large cross sections. A model of deep-inelastic transfer (DIT) for the primary interaction stage and the statistical evaporation code GEMINI for the deexcitation stage have been used to describe the properties of the product distributions. The results have also been compared with the EPAX parametrization of high-energy fragmentation yields. The experimental data show an enhancement in the production of neutron-rich isotopes close to the projectile, relative to the predictions of DIT/GEMINI and the expectations of EPAX. We attribute this enhancement mainly to the effect of the extended neutron distribution (neutron “skin”) of the  $^{64}\text{Ni}$  target in peripheral interactions of  $^{86}\text{Kr}$  with  $^{64}\text{Ni}$ . The large cross sections of such reactions near the Fermi energy, involving peripheral nucleon exchange, suggest that, not only the N/Z of the projectile and the target, but also the N/Z distribution at the nuclear surface may properly be exploited in the production of neutron-rich rare isotopes. This synthesis approach may offer a fruitful pathway to extremely neutron-rich nuclei, towards the neutron-drip line.

*Key words:* Rare isotope production, nuclear reactions, deep inelastic transfer, Fermi energy, neutron “skin”

*PACS:* 25.70.-z, 25.70.Hi, 25.70.Lm

---

<sup>1</sup> E-mail address: soulioti@comp.tamu.edu (G.A. Souliotis).

## 1 Introduction

Synthesis and investigation of very neutron-rich nuclides are of exceptional importance to advance our understanding of nuclear structure and properties at the extreme isospin limit of the nuclear landscape. Many of these nuclides play a key role in stellar nucleosynthesis, especially in the r-process. The production and separation of these nuclides represent an essential ingredient in regards to current or future radioactive beam facilities (see e.g. [1,2]).

Fission or spallation are prolific ways to generate a variety of neutron-rich nuclides (see e.g. [3,4]). In addition, projectile fragmentation of n-rich beams [4] at high or intermediate energy (well above the Fermi energy) has been efficiently employed to produce radioactive beams of n-rich nuclei. The so-called “cold” projectile fragmentation has been described by abrasion/ablation models which provide a phenomenological basis for extrapolation to even more exotic n-rich species [5]. Based on available fragmentation data, a detailed parametrization of the fragmentation cross sections from high-energy reactions has been developed [6] and is commonly used for planning of radioactive beam experiments. In high or medium energy projectile fragmentation reactions, the production of n-rich rare isotopes is based on a more or less “clean-cut” removal of protons from the projectile. In such reactions, the target has almost no effect on the production cross sections, apart from a geometric factor. One-neutron pick-up products are produced with very small cross sections [7].

In contrast to high-energy reactions, the effect of the target neutron-to-proton ratio ( $N/Z$ ) in n-rich rare isotope production has been shown in multinucleon transfer reactions close to the Coulomb barrier. For example, large cross sections for several neutron pick-up channels, along with proton stripping channels have been observed in the reaction of  $^{64}\text{Ni}$  projectiles with  $^{238}\text{U}$  above the Coulomb barrier [8]. The effect of the projectile and target  $N/Z$  in the production of projectile-like fragments from  $^{32,34}\text{S}$  ( $E/A=6-20$  MeV/nucleon) on  $^{12}\text{C}$  and  $^{197}\text{Au}$  has recently been reported in [9], following earlier work in this energy range [10,11]. Deep inelastic collisions around the Coulomb barrier have also been used to produce and study n-rich rare earth isotopes at high spin states [12]. Around the Fermi energy (20–40 MeV/nucleon) a number of n-rich yield measurements of heavy projectiles (e.g.  $^{40}\text{Ar}$ ,  $^{86}\text{Kr}$ ) exist in the literature [13,14], but in these measurements no production cross sections have been reported. Cross sections have been reported for the reaction 70 MeV/nucleon  $^{86}\text{Kr} + ^{27}\text{Al}$  [15], but the n-rich side of the fragment distribution was not covered.

In the present work, we have performed a systematic high-resolution spectrometric study of the production cross sections and the velocity distributions of projectile-like fragments from the reaction 25 MeV/nucleon  $^{86}\text{Kr} + ^{64}\text{Ni}$

with particular attention on the n-rich nuclides. In this study, we observed enhanced production cross sections of n-rich fragments near the projectile and the formation of several neutron pick-up products, along with proton stripping products. The paper is organized as follows: Section 2 describes the experimental setup, the measurements and the data analysis procedures. In Section 3, the experimental results are presented and compared with model predictions. Finally, in Section 4, a summary and conclusions are given.

## 2 Experimental Method and Data Analysis

The present study was performed at the Cyclotron Institute of Texas A&M University. A 25 MeV/nucleon  $^{86}\text{Kr}^{22+}$  beam from the K500 superconducting cyclotron, with a typical current of  $\sim 5$  pA, interacted with an isotopically enriched (98%)  $^{64}\text{Ni}$  target of thickness 4 mg/cm<sup>2</sup>. The reaction products were analyzed with the MARS recoil separator [16]. The primary beam struck the target at 0° relative to the optical axis of the spectrometer. The direct beam was collected in a small square Faraday cup approx. 30 cm after the target, blocking the angular range 0.0–1.0°. The fragments were accepted in the remaining angular opening of MARS: 1.0–2.7° (the angular acceptance of MARS is 9 msr [16]). This angular range lies inside the grazing angle of 3.6° [17] for the present reaction. An Al foil (1 mg/cm<sup>2</sup>) was positioned after the Faraday cup to reset to equilibrium the ionic charge states of the reaction products. MARS optics [16] provides one intermediate dispersive image and a final achromatic image (focal plane) and offers a momentum acceptance of 4%.

At the focal plane, the fragments were collected in a large area (5×5 cm) three-element ( $\Delta E_1$ ,  $\Delta E_2$ , E) Si detector telescope. The  $\Delta E_1$  detector was a position-sensitive Si strip detector of 63  $\mu\text{m}$  thickness whereas the  $\Delta E_2$  and the E detector were single-element Si detectors of 150 and 950  $\mu\text{m}$ , respectively. The position information from the  $\Delta E_1$  strips provided a continuous monitoring of the focusing and collection of the fragments at the various settings of the separator. Time of flight was measured between two PPACs (parallel plate avalanche counters) [18] positioned at the dispersive image and at the focal plane, respectively, and separated by a distance of 13.2 m. The PPAC at the dispersive image was also X–Y position sensitive and used to record the position of the reaction products. The horizontal position, along with NMR measurements of the field of the MARS first dipole, was used to determine the magnetic rigidity  $B\rho$  of the particles. Thus, the reaction products were characterized by an event-by-event measurement of  $dE/dx$ , E, time of flight, and magnetic rigidity. The response of the spectrometer/detector system to ions of known atomic number Z, mass number A, ionic charge q and velocity was calibrated using low intensity primary beams of  $^{40}\text{Ar}$ ,  $^{44}\text{Ca}$  and  $^{86}\text{Kr}$  at 25

MeV/nucleon. To cover the N/Z and velocity range of the fragments, a series of measurements was performed at overlapping magnetic rigidity settings in the range 1.6–2.0 Tesla-meters.

The determination of the atomic number Z was based on the energy loss of the particles in the first  $\Delta E$  detector [19] and their velocity, with a resulting resolution (FWHM) of 0.5 Z units for near-projectile fragments. The ionic charge  $q$  of the particles after the Al stripper, was obtained from the total energy  $E_{tot} = \Delta E_1 + \Delta E_2 + E$ , the velocity and the magnetic rigidity according to the expression:

$$q = \frac{3.107}{931.5} \frac{E_{tot}}{B\rho(\gamma - 1)} \beta\gamma \quad (1)$$

where  $E_{tot}$  is in MeV,  $B\rho$  in Tm,  $\beta = v/c$  and  $\gamma = 1/(1 - \beta^2)^{\frac{1}{2}}$ . The measurement of the ionic charge  $q$  had a resolution of 0.4 units (FWHM). Since the ionic charge must be an integer, we assigned integer values of  $q$  for each event by putting windows ( $\Delta q = 0.4$ ) on each peak of the  $q$  spectrum. Using the magnetic rigidity and velocity measurement, the mass-to-charge A/ $q$  ratio of each ion was obtained from the expression:

$$A/q = \frac{B\rho}{3.107\beta\gamma} \quad (2)$$

Combining the  $q$  determination with the A/ $q$  measurement, the mass A was obtained as:

$$A = q_{int} \times A/q \quad (3)$$

( $q_{int}$  is the integer ionic charge determined as above) with an overall resolution (FWHM) of about 0.6 A units (Fig. 1).

Combination and appropriate normalization of the data at the various magnetic rigidity settings of the spectrometer provided fragment distributions with respect to Z, A,  $q$  and velocity. Correction of missing yields caused by charge changing at the PPAC (positioned at the dispersive image) was performed based on the equilibrium charge state prescriptions of Leon et. al. [20]. (The overall data reduction procedure was similar to that followed in earlier work on  $^{197}\text{Au}$  fragmentation and was described in detail in [21].) The distributions were subsequently summed over all values of  $q$ . It should be pointed out that the resulting distributions in Z, A and velocity are the fragment yield distributions in the reaction angle interval 1.0–2.7° in the magnetic rigidity range 1.6–2.0 Tm. Fig. 1 shows, as an example, the mass spectrum of Germanium (Z=32) isotopes in full resolution.

### 3 Results and Discussion

The gross features of the distributions of projectile fragments from the present reaction are described in Fig. 2. The detailed mass distributions of elements  $Z=35$  to  $Z=30$  are presented in Fig. 3. Before further discussion of the data, we will give an outline of the calculations we performed for this reaction using a phenomenological model appropriate for this energy regime.

The primary interaction stage was modeled with the deep inelastic transfer code of Tassan-Got and Stephan [22] in which stochastic nucleon exchange was assumed for the orbital angular momentum range  $\ell=100$ – $520$ . This DIT model has been successfully applied to describe the primary interaction stage in studies of projectile multifragmentation of  $^{28}\text{Si}$  on  $^{112,124}\text{Sn}$  around the Fermi energy [23]. Events corresponding to trajectories in which the projectile–target overlap exceeded 3 fm were rejected. Following the creation of the primary fragments by the DIT mechanism, the statistical de-excitation of the excited primary fragments was simulated using GEMINI [24]. This statistical deexcitation code uses Monte Carlo techniques and the Hauser-Feshbach formalism to calculate the probabilities for fragment emission with  $Z\leq 2$ . Heavier fragment emission probabilities are calculated using the transition state formalism of Moretto [25]. In the GEMINI calculations, we used Lestone’s temperature dependent level density parameter [26], a fading of shell corrections with excitation energy and we enabled IMF emission. Each partial-wave distribution was appropriately weighted and combined to give the overall fragment A, Z and velocity distributions. The results of the DIT/GEMINI calculation were also filtered by the angular and  $B\rho$  acceptance of the spectrometer. The predictions of this calculation are compared with the present data in the following paragraphs.

In Fig. 2a the mass yield curve is presented. The measured data, normalized for beam current and target thickness are given in mb and presented as open circles. The result of the DIT/GEMINI calculation, filtered by the spectrometer acceptance is given by the dashed line, whereas the full line gives the total (unfiltered) yield. A comparison of the measured yields (open symbols) to the calculated filtered yields (dashed line) shows excellent agreement for the heavier fragments ( $A>65$ ). The discrepancies for lower mass fragments are mainly due to incomplete coverage of the measured data for this mass range. Using the ratio of filtered to unfiltered calculated yield for each mass, correction factors (whose magnitude is inferred from Fig. 2a) for the acceptance of the spectrometer were obtained as a function of mass and were applied to the measured yield data to obtain the total yield, given by the full circles in Fig. 2a. The systematic uncertainty in the extraction of absolute cross sections by this procedure is estimated to be about 40% (FWHM). The correction factors were also employed to obtain total isotope production cross sections (Fig. 3)

from the measured yields. A comparison of the extracted total isobaric cross sections (full circles) to the calculated unfiltered yields (full line) again shows fair agreement, except for the lower mass fragments ( $A < 65$ ).

In Fig. 2b, the measured yield distributions as a function of  $Z$  (relative to the line of  $\beta$  stability,  $Z_\beta$ ) and  $A$  are presented as contour lines. The line of stability is calculated as:  $Z_\beta = A/(1.98 + 0.0155A^{2/3})$  [27]. The calculated values from DIT/GEMINI are shown as a thick full line (without acceptance cut) and as a thick dashed line (with spectrometer acceptance cut). The thin dashed line is from the EPAX parametrization [6] of relativistic fragmentation data and is given here for comparison. From this Figure we see that very neutron-rich nuclides (up to 4  $Z$  units away from stability for isobars near the projectile) are produced. The DIT/GEMINI calculation describes reasonably well the experimental data. Finally, the locus of the relativistic fragmentation data is towards more proton-rich fragments than the data in this energy regime.

Finally, in Fig. 2c, the velocity vs. mass distributions are given. The data are again shown as contours. The thick full line is from the DIT/GEMINI calculation without acceptance cut and the dashed line is with acceptance cut. This mass resolved velocity distribution exhibits correlations characteristic of quasi-elastic interactions (for near projectile fragments) and deep inelastic interactions (for fragments further away from the projectile) as revealed by the continuous fragment ridge with monotonically decreasing velocities. For lower masses ( $A < 65$ ) the fragment velocities seem to increase with decreasing mass. This is due to the fact that the spectrometer settings were such that only forward moving fragments coming from decay of highly excited primary products were observed. In addition, comparing the filtered DIT/GEMINI calculations with the data, we see that the calculation is able to describe well the observed velocity distributions in the whole mass range. In summary, based on the comparisons presented in Fig. 2, we can state that the DIT/GEMINI calculation is able to provide a satisfactory quantitative description of the observed gross distributions. Also, as we will see below, it does a fair job in predicting the absolute values of the production cross sections (except for the very n-rich isotopes, as will be pointed out).

In Fig. 3, the mass distributions for elements  $Z=35-30$  are presented. In this figure, the full circles are the present data, corrected for the spectrometer acceptance as discussed earlier. The open squares are the predictions of the DIT/GEMINI calculation. The dotted lines are the predictions of the EPAX parametrization [6] of relativistic fragmentation cross sections and are plotted here for comparison. Note that, in high-energy fragmentation, nucleon-pickup products are not produced or, at best, are highly suppressed compared to lower energy peripheral collisions [7]. As we see, neutron-rich nuclides are produced with large cross sections. Apart from proton-removal products, neutron pick-up fragments are produced. For example, for the case of selenium ( $Z=34$ ),

which corresponds to the removal of 2 protons from the projectile, up to 4 neutrons are seen to be picked-up to produce  $^{88}\text{Se}$  (with cross section of  $0.3 \mu\text{b}$ ). Similarly, for germanium (four-proton-removal from the projectile), up to two neutrons are picked-up to give  $^{84}\text{Ge}$  (cross section  $0.4 \mu\text{b}$ ).

For near-projectile elements, an enhanced production of neutron rich isotopes is observed relative to the expectations of the EPAX parametrization. Also, the DIT/GEMINI calculation, while able to describe rather well the n-deficient and the central part of the distributions, fails to describe the n-rich sides of the distributions for elements above zinc ( $Z=30$ ). Since this enhancement is observed for near projectile elements, it should be a result of very peripheral collisions, where the nucleon exchange is restricted near the surface of the projectile and the target. To further examine this statement, we present in Fig. 4 the velocity distributions for elements  $Z=35-30$ . These distributions have two components: a narrow one peaking close to the beam velocity (quasielastic) and another wider component peaking at lower velocity (deep inelastic component). The quasielastic component progressively decreases for fragments with lower  $Z$ . As expected, the production of the most neutron-rich isotopes is associated with the quasielastic component (also verified in two-dimensional correlations of  $A$  with velocity). Using velocity vs impact parameter correlation from the DIT/GEMINI calculation, we found that these peripheral events correspond to a projectile–target overlap not exceeding 1–1.5 fm.

Qualitatively, the enhanced production of neutron rich fragments from  $^{86}\text{Kr}$  may be understood by considering the peripheral character of the collisions and the particular structure of the projectile and the target. The projectile has a compact neutron distribution ( $N=50$  closed shell) and, reversely, the target has a compact proton distribution ( $Z=28$  closed shell) and a more diffuse neutron distribution ( $N=36$ , partially filled neutron shell with 8 neutrons above the closed shell  $N=28$ ). In peripheral collisions, an overlap of the  $^{86}\text{Kr}$  projectile surface with the neutron-rich  $^{64}\text{Ni}$  surface (neutron “skin”) will lead to a local nucleon redistribution and  $N/Z$  equilibration, favoring the production of more neutron-rich fragments near the projectile. For larger projectile–target overlaps this effect washes out and the observed fragments have more or less cross sections as described by DIT/GEMINI. Interestingly, they are in general agreement with EPAX, despite the vastly different primary interaction mechanism, indicating that such products result from long evaporation chains of highly excited primary nuclei. It should be noted that in the DIT code, the nuclei are assumed spherical with homogeneous proton and neutron density distributions. Incorporating realistic proton and neutron density distributions in the DIT code may improve the capability to describe peripheral collisions in projectile–target combinations where the neutron–proton profile of nuclear surface can play a role, as in the present case of the  $^{86}\text{Kr}+^{64}\text{Ni}$  system.

From a practical standpoint, the large production cross section of neutron-

rich nuclides, and more importantly the neutron pick-up possibility can render these reactions a useful route to produce extremely neutron-rich nuclides. It may be noted that neutron pick-up cross sections are also large in the case of multinucleon transfer reactions close to the Coulomb barrier [8]. However, these reactions have very wide angular, velocity and ionic charge distributions, in addition to the necessity of rather thin targets (around 1 mg/cm<sup>2</sup>). Around the Fermi energy, however, inverse kinematic reactions have angular and ionic charge state distributions that can be efficiently dealt with using a large acceptance spectrometer (e.g. MARS in the present study). Also the energies are high enough to allow moderately thick targets (10–30 mg/cm<sup>2</sup>).

Using the present cross sections, we can make estimates of rare isotope production rates from intense beams at this energy regime. As examples, we present in Table I the cross sections and production rates for the most n-rich nuclides of Se (Z=34) and Ge (Z=32). The experimental cross sections of this work are given in the second column, while the the third column gives the cross sections predicted by the DIT/GEMINI calculation. The fourth column gives the cross sections measured in the reaction <sup>86</sup>Kr(500 MeV/nucleon) + Be [7]. We observe, as already discussed, the inability of the present simulation to reproduce the measured cross sections of the most n-rich nuclides. Also, we note that in relativistic peripheral collisions, up to one neutron can be picked up from the target with very low cross section. The rates given in the last column of the table were calculated using the measured cross sections and assuming a beam of 100 pA <sup>86</sup>Kr at 25 MeV/nucleon striking a 20 mg/cm<sup>2</sup> <sup>64</sup>Ni target. Such yields of very neutron rich isotopes may enable a variety of nuclear structure and nuclear reaction studies in the Fermi energy regime. These rare isotopes may be separated in flight with a large acceptance separator or can be stopped and collected in a gas cell with the possibility of subsequent charge breeding and reacceleration [28].

Finally, another interesting possibility is the use of such reactions as a second stage in two-stage rare isotope production schemes. For example, a beam of <sup>90</sup>Kr from an ISOL facility can be accelerated around the Fermi energy and subsequently strike a <sup>64</sup>Ni target to produce very n-rich nuclides that may be separated and studied in flight. To estimate the rates of such reaction products the present cross sections can be used as a first approximation. However, a quantitative prediction will be possible after improving our present description of these peripheral collisions between n-rich nuclei.

## 4 Summary and conclusions

In the present study, the yields and velocity distributions of projectile-like fragments from the reaction of 25 MeV/nucleon <sup>86</sup>Kr + <sup>64</sup>Ni were measured using



the MARS recoil separator at Texas A&M, with special focus on the neutron rich isotopes. Proton-removal and neutron pick-up isotopes have been observed with substantial cross sections. A model of deep-inelastic transfer (DIT) for the primary interaction stage and the statistical evaporation code GEMINI for the deexcitation stage have been used to describe the properties of the product distributions. The results have also been compared with the high-energy fragmentation parametrization EPAX. The experimental data show an enhancement in the production of n-rich isotopes close to the projectile relative to the predictions of DIT/GEMINI and the expectations of EPAX. We attributed this enhancement to the effect of the target  $^{64}\text{Ni}$  neutron “skin” in peripheral interactions of  $^{86}\text{Kr}$  with  $^{64}\text{Ni}$ . The large cross sections of such reactions near the Fermi energy, involving peripheral nucleon exchange between the projectile and the target, suggest that not only the N/Z of the projectile and the target, but also the N/Z distribution at the surface (i.e. neutron “skin”) may be properly exploited in the production of rare neutron-rich isotopes. This synthesis approach may provide a fruitful pathway to extremely neutron rich nuclei towards the neutron-drip line.

## 5 Acknowledgement

We would like to thank A. Sanzhur for useful discussions regarding neutron density distributions and relevant calculations. We gratefully acknowledge the support of the operations staff of the Cyclotron Institute during the measurements. Financial support for this work was given, in part, by the U.S. Department of Energy under Grant No. DE-FG03-93ER40773 and by the Robert A. Welch Foundation under Grant No. A-1266.

## References

- [1] Long-Range Plan for Nuclear Physics (1996), DOE–NSF Nucl. Sci. Advisory Committee, accessible at [www.er.doe.gov/production/henp/np/nsac/lrp.html](http://www.er.doe.gov/production/henp/np/nsac/lrp.html).
- [2] Radioactive Nuclear Beam Facilities, NuPECC Report, April 2000; see also EURISOL web page: [www.ganil.fr/eurisol/](http://www.ganil.fr/eurisol/)
- [3] H. Geissel and G. Munzenberg, *Annu. Rev. Nucl. Part. Sci.* 45 (1995) 163.
- [4] D.J. Morrissey and B. M. Sherrill, *Phil. Trans. R. Soc. Lond. A* 356 (1998) 1985.
- [5] W.A. Friedman, M.B. Tsang, D. Bazin, and W.G. Lynch, *Phys. Rev. C* 62 (2000) 064609-1.

- [6] K. Summerer and B. Blank, Phys. Rev. C61 (2000) 034607.
- [7] M. Weber et al., Nucl. Phys. A578 (1994) 659.
- [8] L. Corradi et al., Phys. Rev. C 59 (1999) 261.
- [9] O.B. Tarasov et al., Nucl. Phys. A629 (1998) 605.
- [10] A.G. Artukh et al., Nucl. Phys. A 176 (1971) 284.
- [11] V.V. Volkov, Phys. Rep. 44 (1978) 93.
- [12] I.Y. Lee et al., Phys. Rev. C 56 (1997) 753.
- [13] Ch.O. Bacri et al., Nucl. Phys. A 555 (1993) 477.
- [14] D. Bazin et al., Nucl. Phys. A 515 (1990) 349.
- [15] R. Pfaff et al., Phys. Rev. C51 (1995) 1348.
- [16] R.E. Tribble, R.H. Burch and C.A. Gagliardi, Nucl. Instr. and Meth. A 285 (1989) 441.
- [17] W.W. Wilcke et al., At. Data Nucl. Data Tables **25**, 389 (1980).
- [18] G. Chubarian, private communication.
- [19] F. Hubert, R. Bimbot and H. Gauvin, Atom. Data and Nucl. Data Tables 46 1 (1990) and Nucl. Instrum. Methods B36 (1989) 357.
- [20] Leon et al., At. Data Nucl. Data Tables 69 (1998) 217.
- [21] G.A. Souliotis et al., Phys. Rev. C57 (1998) 3129.
- [22] L. Tassan-Got, and C. Stefan, Nucl. Phys. A524 (1991) 121.
- [23] M. Veselsky et al., Phys. Rev. C62 (2000) 064613.
- [24] R. Charity, et al., Nucl. Phys. A483 (1988) 391. The version of GEMINI included modifications made up to July, 1998.
- [25] L.G. Moretto, Nucl. Phys. A247 (1975) 211.
- [26] J. Lestone, Phys. Rev. C52 (1995) 118.
- [27] P. Marmier and E. Sheldon, Physics of Nuclei and Particles, Volume I (Academic, New York, 1970) p. 15.
- [28] "A Proposed Facility Upgrade for the Texas A&M Univ. Cyclotron Institute", accessible at: [http://cyclotron.tamu.edu/facility\\_upgrade.htm](http://cyclotron.tamu.edu/facility_upgrade.htm)

Table 1

Cross sections and rates (last column) of Se and Ge isotopes from  $^{86}\text{Kr}$  fragmentation. For the rates, the cross section data of this work are used and a primary beam of  $^{86}\text{Kr}$  (25 MeV/nucleon) of intensity 100 pnA is assumed to interact with a  $^{64}\text{Ni}$  target of  $20 \text{ mg/cm}^2$  thickness (see text).

Rare Isotope:	Reaction channel	Cross Sections			Rate ( $\text{sec}^{-1}$ )
		Experiment: This work	Calculated DIT/GEMINI	High Energy Data [7]	
$^{84}\text{Se}$	-2p+0n	4.7 mb	0.8 mb	2 mb	$5.6 \times 10^5$
$^{85}\text{Se}$	-2p+1n	$900 \mu\text{b}$	$60 \mu\text{b}$	$8 \mu\text{b}$	$1.1 \times 10^5$
$^{86}\text{Se}$	-2p+2n	$100 \mu\text{b}$	$3 \mu\text{b}$	–	$1.2 \times 10^4$
$^{87}\text{Se}$	-2p+3n	$14 \mu\text{b}$	–	–	$1.7 \times 10^3$
$^{88}\text{Se}$	-2p+4n	$0.3 \mu\text{b}$	–	–	$3 \times 10^1$
$^{82}\text{Ge}$	-4p+0n	$22 \mu\text{b}$	$2 \mu\text{b}$	$3 \mu\text{b}$	$2.6 \times 10^3$
$^{83}\text{Ge}$	-4p+1n	$2.3 \mu\text{b}$	–	$0.04 \mu\text{b}$	$2.8 \times 10^2$
$^{84}\text{Ge}$	-4p+2n	$0.4 \mu\text{b}$	–	–	$4.8 \times 10^1$

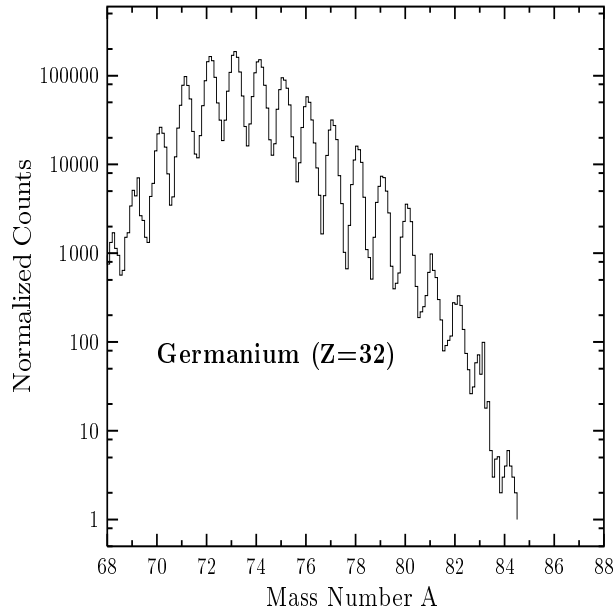


Fig. 1. Mass histogram of Germanium ( $Z=32$ ) isotopes

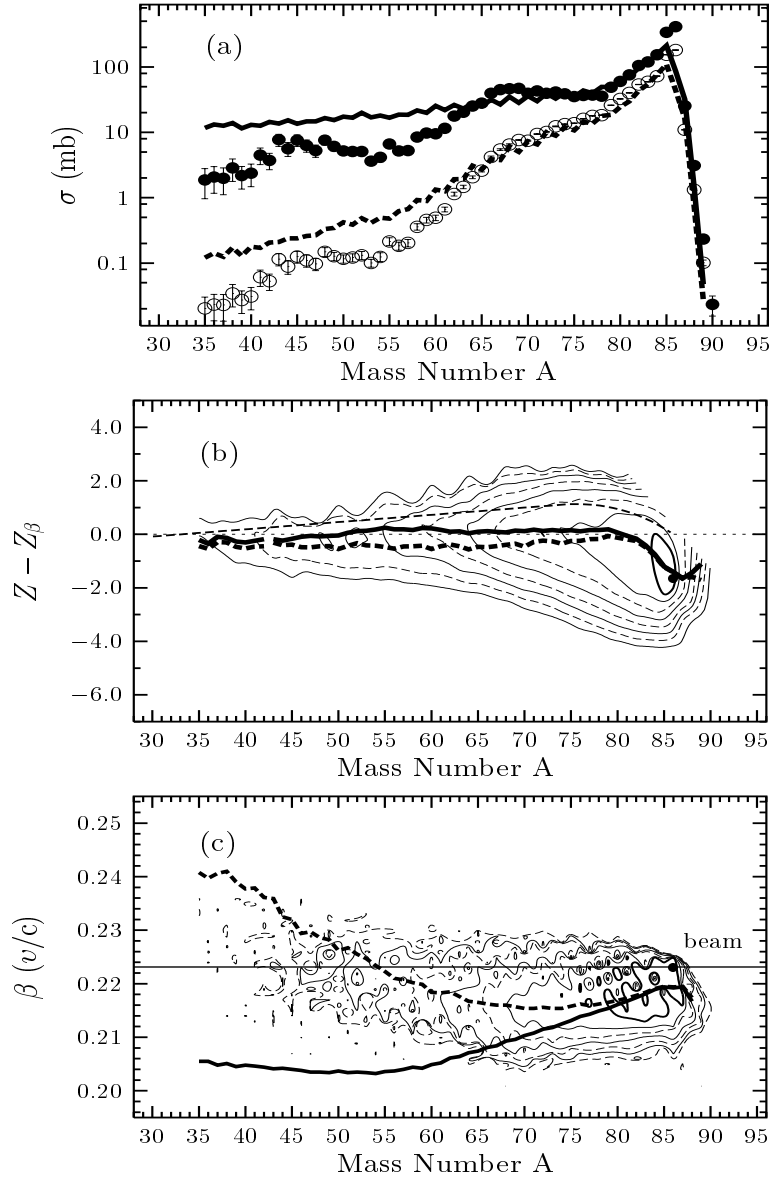


Fig. 2. Fragment distributions for the reaction 25 MeV/nucleon  $^{86}\text{Kr} + ^{64}\text{Ni}$ . (a) - isobaric yield distribution. The data are shown as solid circles (total cross sections) and open circles (with acceptance cut). The full line is the result of DIT/GEMINI (see text). The dashed line is the result of the same calculation as the full line, but with a cut corresponding to the angular and momentum acceptance of the spectrometer. (b) - yield distributions as a function of  $Z$  (relative to the line of  $\beta$  stability,  $Z_\beta$ ) and  $A$ . Highest yield contours are plotted with thicker lines. Successive contours correspond to a decrease of the yield by a factor of 2. The calculated values from DIT/GEMINI are shown as i) thick full line: without acceptance cut and, ii) thick dashed line: with acceptance cut. Thin dashed line: EPAX parametrization. (c) - velocity vs. mass distributions. Data are shown as contours as in (b). The thick lines are as in (b). The horizontal full line represents the beam velocity.

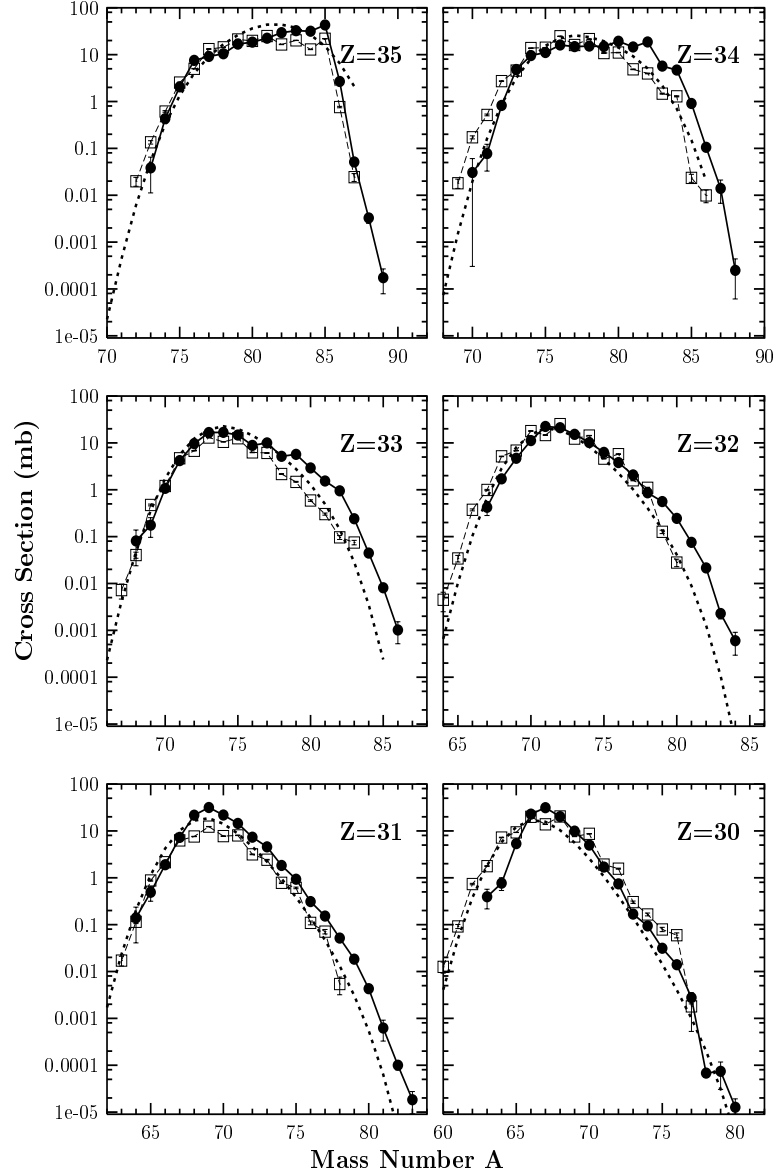


Fig. 3. Mass distributions of several elements from the reaction of 25 MeV/nucleon  $^{86}\text{Kr}$  with  $^{64}\text{Ni}$ . The present data are shown by full circles. Open squares are simulations according to DIT/GEMINI and the dotted line is from the high-energy parametrization EPAX (see text).

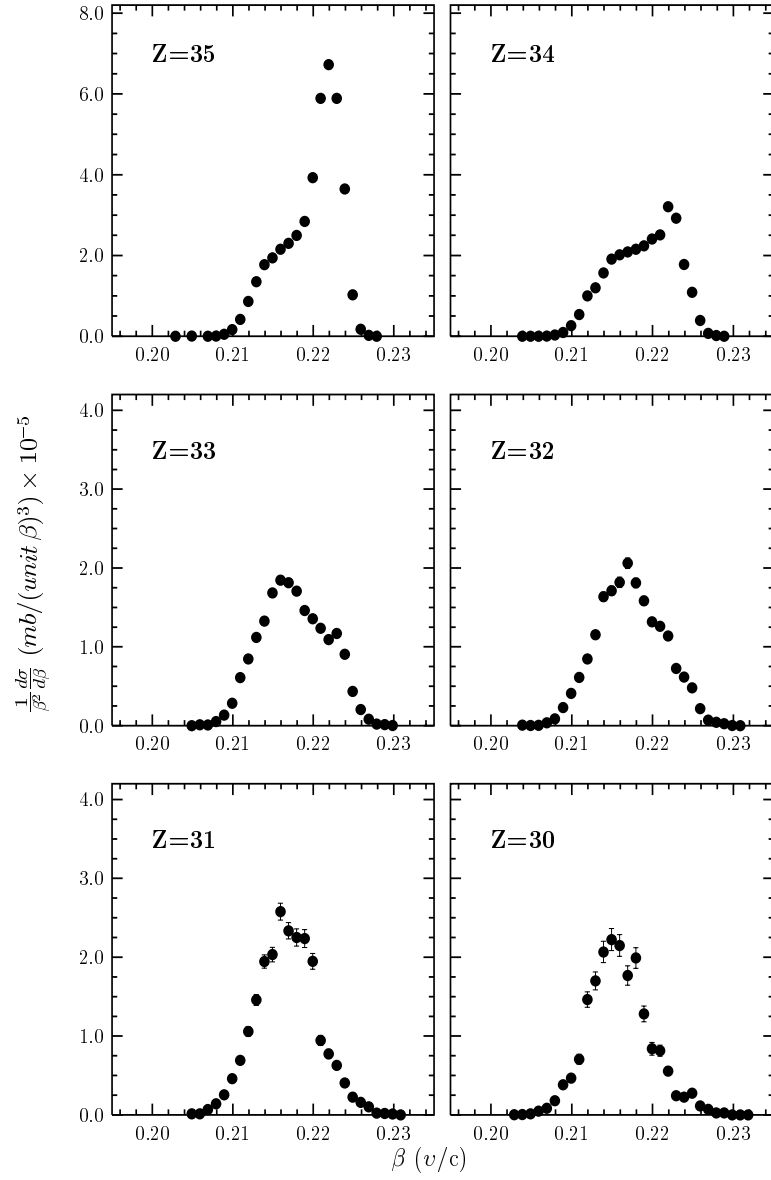


Fig. 4. Velocity distributions for elements Z=35–30 (see text).